논문

Characteristics of Supersonic Jet Impingement on a Flat Plate

Seung-kyu Hong*1, Kwang-Seop Lee*1, Seung-O Park*2

평판에 충돌하는 초음속 제트에 유동특성

홍승규, 이광섭, 박승오

Viscous solutions of supersonic jet impinging on a flat plate normal to the flow are simulated using three-dimensional Navier-Stokes solver. The jet impinging flow structure exhibits such complex nature as shock shell, plate shock and Mach disk depending on the flow parameters. Among others, the dominant parameters are the ratio of the nozzle exit pressure to the ambient pressure and the distance between the nozzle exit plane and the impinging plane. In the present study, the nozzle contour and the pressure ratio are held fixed, while the jet impinging distance is varied to illuminate the characteristics of the jet plume with the distance.

As the plate is placed close to the nozzle at 3D high, the computed wall pressure at or near the jet center oscillates with large amplitude with respect to the mean value. Here D is the nozzle exit diameter. The amplitude of wall pressure fluctuations subsides as the distance increases, but the maximum mean pressure level at the plate is achieved when the distance is about 4D high. The frequency of the wall pressure is estimated at 6.0 kHz, 9.3 kHz, and 10.0 kHz as the impinging distance varies from 3D, 4D, to 6D, respectively.

Key Words: Supersonic Jet Impingement, Nozzle Flow, Barrel Shock, CFDS Method

1. Introduction

Supersonic jet occurs in the exhaust from rocket motors and from V/STOL aircraft engines and its interaction is found in various situations such as multistage rocket separation and flame deflectors of missiles, among others. When these jets impinge on bottom of a missile launcher or the ground surface, high level of heat flux and pressure loads can be generated.

* 2001년 6월 16일 접수

*1 정회원, 국방과학연구소 3체계-2-1

*2 정회원, 한국과학기술원

These impinging flows are generally found to be quite complex. The main applications of this problem include prediction of surface erosion and design of launcher systems. The key features of the flow field are plate shock, barrel shock, and jet boundary. Embedded between the plate shock and the solid surface is a region of subsonic and transonic flows similar to that found in the stagnation zone of blunt body in supersonic flow. Structure of this type of jet has been examined for many years both experimentally [1]-[14] and numerically [15]-[23].

While most of existing studies are confined to 2-D axisymmetric flows, Hong and Lee [20] presented numerical simulations of jet plume

impingement onto a deflecting duct using Navier-Stokes equations. Lee et al. [21] also gave numerical solutions for a VLS-type missile launcher tube involving supersonic jet impingement. These flow patterns are extremely complex and hard to obtain stable numerical solutions [22].

In particular Sakakibara and Iwamoto [23] investigated oscillatory mechanism associated with under-expanded jet impinging on a plate. They have identified pressure oscillation, frequency, and separation bubble on the plate for different nozzle-plate distances. It is this kind of oscillatory behavior that is also observed in the present study that will be highlighted.

Having observed this, objectives of present numerical study are thus two folds: one is to capture unsteady nature of jet impingement structure while the jet undergoes a transitory process, the other is to overcome the inherent shock instability problem associated with Roe scheme to which the present CFDS scheme owes its ideas. Present work in particular focuses on the change of jet impingement structure as the distance between the nozzle exit plane and the flat plate varies between 3 to 6 nozzle exit diameters. Analysis and prediction techniques of this jet impingement process can be directly extended to designing three-dimensional, complex Vertical Launching System (VLS) flame deflector, for which one needs to know the exhaust flow pattern as well as the level of maximum pressure, temperature and heat flux rate. Presently analysis, design and manufacturing of VLS launcher are under way.

2. Numerical Method

The governing Navier-Stokes equations employed in the generalized coordinate system, (ξ, η, ϕ), are expressed for the conservative variable vector as

$$J^{-1}\frac{\partial q}{\partial t}+\frac{\partial}{\partial \xi}(\hat{F}+\hat{F}_v) +\frac{\partial}{\partial \eta}(\hat{G}+\hat{G}_v)+\frac{\partial}{\partial \phi}(\hat{H}+\hat{H}_v)=0 \quad (1)$$

The inviscid fluxes are linearized and split for upwind discretizations by

$$\triangle_\xi F=\hat{A}\triangle q=(\hat{A}^+ +\hat{A}^-)\triangle q \quad \text{and}$$

$$\hat{A}^{\pm}=\overline{M}\,\overline{T}\,\overline{\Lambda}^{\pm}\,\overline{T}^{-1}\,\overline{M}^{-1} \quad (2)$$

yielding

$$J^{-1}\delta q+\hat{A}^+\nabla_\xi q+\hat{A}^-\triangle_\xi q +\hat{B}^+\nabla_\eta q+\hat{B}^-\triangle_\eta q +\hat{C}^+\nabla_\phi q+\hat{C}^-\triangle_\phi q=0 \quad (3)$$

where $\delta q=q^{n+1}-q^n$. The strength of current formulation, termed as Characteristic Flux Difference Splitting (CFDS) scheme, is to enable one to switch the difference equation from the conservation form

$$\frac{J}{\Delta t}\delta q+\overline{MT\Lambda}\,\overline{T}^{-1}\,\overline{M}^{-1}\Delta q=0 \quad (4)$$

to characteristic form

$$\frac{J}{\Delta t}\delta\tilde{q}+\overline{\Lambda}\Delta\tilde{q}=0 \quad (5)$$

at the boundary for application of implicit characteristic boundary conditions. Details of formulation and its applicability to characteristic boundary procedure are given in Ref. 24.

When the eigenvalue becomes zero in Eq. (5), there is no convective wave information traveling to that point as occurs in the stagnation line. Since the CFDS formulation also splits the eigenvalue as

$$\Lambda=\Lambda^+ +\Lambda^- \quad (6)$$

this splitting is also susceptible to carbuncle problem when λ_1 becomes zero. When the velocity component parallel to the shock becomes zero, the associated eigenvalue matrix becomes

$$\overline{\Lambda} \cong \begin{bmatrix} u & & & & & \\ & u & & & & \\ & & u & & & \\ & & & u+c & & \\ & & & & u-c & \end{bmatrix} \quad (7)$$

$$= \begin{bmatrix} 0 & & & & & \\ & 0 & & & & \\ & & 0 & & & \\ & & & c & & \\ & & & & -c & \end{bmatrix}$$

Thus it is necessary to prevent the eigenvalue component from becoming zero. This can be done via

$$\lambda = \lambda^+ + \lambda^- = (\lambda^+ + \varepsilon) + (\lambda^- - \varepsilon) \quad (8)$$

with a proper choice of ε. Sanders et al [25] recently found the H-correction method work well preventing the bow shock instability via

$$\lambda^H_{j+1/2,k} = \max(\lambda_{j+1/2,k}, \lambda_{j,k+1/2}, \lambda_{j,k-1/2}, \lambda_{j+1,k+1/2}, \lambda_{j+1,k-1/2})$$

However, the shock instability occurs for 3-dimensional shock flows even if the entropy fixing is imposed as proposed by ether Harten or Sanders.

An alternative formulation of the flux term instead of Eq. (2) is employed in the grid-aligned shock area:

$$\triangle_\xi F = Flux_{\frac{1}{2}} - Flux_{-\frac{1}{2}} \quad (9)$$

where

$$Flux_{\frac{1}{2}} = \frac{1}{2}[F_j + F_{j+1} - |\hat{A}|(Q_{j+1} - Q_j)] \quad (10)$$

Here, $\hat{A}$ is the same as in Eq. (2). The last term in Eq. (10), $|\hat{A}|(Q_{j+1} - Q_j)$, means numerical dissipation and $|\hat{A}| = \overline{M}\,\overline{T}\,|\overline{\Lambda}|\,\overline{T}^{-1}\,\overline{M}^{-1}$. The flux definition in Eq. (10) is similar in form to the Roe's flux definition. In the present study for supersonic jet impingement calculations, the entropy fixing formula in Eq. (10) takes

$$|\lambda| = \left(\frac{\lambda^2 + \varepsilon^2}{2\varepsilon}\right) \quad \text{if } |\lambda| < \varepsilon, \text{ and} \quad (11)$$

with $\varepsilon = 2.0$.

This entropy fixing is applied when one detects the normal shock aligned with grid. The formulation in Eq. (2) is restored in the rest of the flow field. It is this reason that the present computation utilized the 3-D code for analysis of axi-symmetric jet impingement flow to see if the present fix, Eqs. (9)-(11), is able to capture unsteady plate shock. Another reason is that the present code is used to simulate the complex 3-D, VLS-type launcher for which we also have obtained satisfactory numerical solutions.

3. Results and Discussions

Supersonic jet impingement cases are run for a nozzle with chamber pressure Pt=1200 psia and chamber temperature Tt=2950 K. Figure 1 shows the computational model with the nozzle diameter of D=32.6 mm, and the nozzle-plate distance of H. The ratio of nozzle exit area to nozzle throat area is 7.38. The computational grid consists of 310000 grid points and of seven blocks. Also overlap grid technique is used at block interfaces. Figure 2 shows grid in symmetric plane and Fig. 3 displays overlapped grid in the core region in transverse plane parallel to the plate. A circle denoted with a solid line in Fig. 3 coincides with the nozzle exit plane in size. This grid system without singular line helps improve solution quality and convergence. The computational domain starts from the nozzle throat with Mach 1.0 condition. The inflow boundary conditions at the nozzle throat are calculated from isentropic relations and perfect gas law. A specific heat ratio of 1.4 is used.

The jet impinging distance H is varied for 3D, 4D, 5D, and 6D to illuminate the characteristics of the jet plume with the distance. Figure 4 shows Mach contours with contaminated shock structure, so-called "carbuncle phenomenon" in symmetric plane. When a supersonic jet plume exhausts onto the plate, strong normal shock is formed above the

plate. Since the grid system used in numerical computation is aligned with this normal shock, it is known to cause the shock instability [26,27]. This shock instability is cured by fixing near-zero eigenvalues through the numerical dissipation term. Figure 5 exhibits Mach contours displaying shock shell, plate shock and Mach disk for various H. Those structures are not settled fully. Rather the plate shock in Fig. 5 still bounces up and down while keeping the structure shown in the figure intact. Especially, when the distance is small as in Fig. 5.(a), the plate shock merges with the Mach disk and oscillates more vigorously, yet maintaining its shock structure. As the distance H increases, the shock structures are also stretched; but the distance between the plate and plate shock maintains nearly the same height regardless of H.

Typical pressure distributions on the flat plate are captured in Fig. 6 for H=3D and 4D. The nozzle exit diameter is denoted on the figure with a bold circle to show the extent of highly concentrated wall pressure zone. The labels in Fig. 6 are with respect to the atmospheric pressure. It is noted that pressure contours form exact circles in spite of using the rectangular grid in the core zone.

In the course of computation, it is observed that the plate shock in Fig. 5 moves up and down continuously and the wall pressure fluctuates with respect to a mean value without reaching the steady-state value. This is due to the closeness of the distance between the wall and the nozzle. The high-Mach upstream of the plate shock after passing through the shock has to turn abruptly due to the presence of the plate, causing the flow turn and pressure drop. But once the pressure drops, the plate shock is pushed closer to the wall which makes the pressure high in the trapped zone. This in turn pushes the plate shock move upward again. This cyclic behavior is seen repeatedly,
shown in Fig. 7 in terms of wall pressure fluctuations. Figure 7 represents wall pressure history as a function of numerical iterations. As the plate is placed close to the nozzle, the computed wall pressure in Fig. 7(a) oscillates with large amplitude with respect to the mean value, yet barely maintaining periodicity of wall fluctuations. The amplitude of wall pressure fluctuations decreases as the distance increases, but the maximum mean pressure level at the plate is achieved when the distance is about 4D high. The frequency of the pressure fluctuations could be estimated from Fig. 7. In the steady zone, the frequency ranges from 6.0 kHz, 9.3 kHz and 10.0 kHz as the distance varies from 3D, 4D to 6D, respectively. The frequency is based on the conversion of the numerical iteration to the flow time which in turn is transformed from the CFL number. The CFL number depends on the grid cell spacing. So there is somewhat arbitrariness in converting iteration to the elapsed flow time. Nevertheless it is important to note that the jet impingement process fluctuates with a certain frequency on the order of 6-10 kHz at a close range. Note that the frequency of Sakakibara and Iwamoto [20] is approximately 20 kHz for a different jet condition.

Figure 8 shows heat flux prediction in radial direction for 4D case. Heat flux reaches its peak at X/R=0.8, where R is the radius of the nozzle exit. Peak value occurs off the center which is typical for this type of flow. Qualitative comparison of computed heat flux rate with measured data is planned for our next experiment at ADD. Mean pressure distribution in radial direction in Fig. 9 exhibits typical pattern of supersonic jet impinging on flat plate [8]. In Fig. 9, the measured wall pressure is also denoted with a symbol, showing a good match between the prediction and the measurement. This experiment was done solely to provide the database for our computation and to measure the wall erosion for the ablative material. The pressure history at the center of the plate is presented in Fig. 10 collectively for the four different heights, showing the highest mean pressure occurs when H=4D. The amplitude of pressure

fluctuation subsides as the wall-plate distance increases. Finally, computed thrust of the motor converges rather steadily in Fig. 11 for the four cases, yielding almost the same level of thrust at 300 lbs.

4. Conclusions:

Behavior of the complex, unsteady jet impingement flow is documented during its initial stage. The plate shock has been captured robustly with the addition of numerical dissipation when the shock is aligned with the grid line. The computed wall pressure compares well with the experimental data acquired recently at Anheung Proving Ground. The computational methodology currently applied to simple plate is now extended to the design of complex vertical launcher, yielding the robust numerical solutions near the bottom wall similar to those presented in this paper and thus, setting a foundation to be a stable and viable numerical scheme.

References

[1] Gummer, J. H., and Hunt, B. L., "The Impingement of a Uniform, Axisymmetric, Supersonic Jet on a Perpendicular Flat Plate," Aeronautical Quarterly, Vol. 12, 1971, pp. 403-420.

[2] Donaldson, C. DUP, Snedeker, R. S., "A study of free Jet Impingement. Part 1. Mean properties of free and impinging jets," Journal of Fluid Mechanics, Vol. 45, No. 2, 1971, pp. 281-319.

[3] Knight, C. V., "Experimental Investigation of Two-Dimensional, Supersonic Flow Impingement on a Normal Surface," AIAA Journal, Vol. 11, No. 2, 1973, pp. 233-235.

[4] Kalghatgi, G. T., and Hunt, B. L., "Occurrence of Stagnation Bubble in Supersonic Jet Impingement Flows," The Aeronautical Quarterly, Vol. 27, No. 3, Aug. 1976, pp. 169-185.

[5] Lamont, P. J., and Hunt, B.L., "The Impingement of Underexpanded axisymmetric jets on Wedges," Journal of Fluid Mechanics, Vol. 76, part 2, 1976, pp. 307-336.

[6] Zien, T. F., and Driftmyer, R. T., "Two-Dimensional Supersonic Jet Impingement on a Flat Plate," AIAA Journal, Vol. 17, No. 1, 1979, pp. 4-5.

[7] Pamadi, B. N., "On the Impingement of Supersonic Jet on a Normal Flat Surface," Aeronautical Quarterly, 1982, pp. 199-218.

[8] Lamont, P. J., and Hunt, B.L., "The Impingement of Under-expanded Jet Interaction with a Plane Obstacle," Journal of Fluid Mechanics, Vol. 100, No. 3, 1980, pp. 471-511.

[9] Iwamoto, J., "Impingement of Under-Expanded Jets on a Flat Plate," Journal of Fluid Engineering, Vol. 112, No. 2, June 1990, pp. 179-184.

[10] Masuda, W. and Moriyama, E., "Aerodynamic Characteristics of Under-expanded Coaxial Impinging Jets," JSME International Journal, Series B, Vol. 37, No. 4, 1994, pp. 769-775

[11] Al-Qutub, A. M., and Budair, M. O., "Experiments of the Flow Over a Flat Surface Impinged by a Supersonic jet," AIAA Paper 95-2935.

[12] Alvi, F. S., and Iyer, K. G., "Mean and Unsteady Flowfield Properties of Supersonic Impinging Jets with Lift Plates," AIAA Paper 99-1829, 5th AIAA/CEAS Aeroacoustics Conference, 10-12 May 1999.

[13] 이택상, 박종호, 신필권, 신완순, 김윤곤, "초음속 충돌제트의 유동 특성에 대한 실험적 연구," 한국추진공학회지 제2권 3호, pp. 10-19, 1998

[14] 이택상, 이정민, 신완순, 박종호, 김윤곤, "평판위에 충돌하는 초음속 과소팽창 제트에 관한 실험적 연구," 한국추진공학회지 제3권 3

호, pp. 53-61, 1999.

[15] Rubel, A., "Inviscid Axisymmeetric Jet Impingement with Recirculating Stagnation Regions," AIAA Journal, Vol. 21, No. 3, March 1983, pp. 351-357.

[16] Rizk, M. H. and Menon, S., "Numerical Simulation of Impinging Jets," AIAA 24th Aerospace Science Meeting, Jan.6-9, 1986/Reno, Nevada, AIAA Paper 86-0279

[17] Kim, K. H., and Chang, K. S., "Three-Dimensional Structure of a Supersonic Jet Impinging on an Inclined Plate," Journal of Spacecraft and Rockets, Vol. 31, No.5, Sep.-Oct., 1994, pp. 778-782.

[18] Chow, W. L., Ke, Z. P., and Lu, J. Q., "The Interaction between a Jet and a Flat Plate - an Inviscid Analysis," Journal of Fluids Engineering, Vol. 117, 1995, pp. 623-627.

[19] Kitamura, S., and Iwamoto, J., "Numerical Analysis of Supersonic Impinging Jet," Trans. Japan Soc. Aero. Space Sci. Vol. 41, No. 132, 1998, pp. 57-64.

[20] Sakakibara, Y., and Iwamoto, J., "Numerical Study of Oscillation Mechanism in Uderexpanded Jet Impinging on Plate," Journal of Fluids Engineering, Vol. 120, Sep. 1998, pp. 477-481.

[21] Hong, S. K. and Lee, K. S., "Simulation of Jet Plume Impinging onto a Duct," ISABE 97-7184, AIAA ISOABE (International Society for Air Breathing Engines) Symposium Papers, Sep. 7-12, 1997, Chattanooga, Tenneessee, USA, pp. 1359-1365.

[22] Lee, K. S., Hong, S. K. and Park, S. O., "Internal Flow Characteristics of VLS type Canister," Preceedings of The First National Congress on Fluids Engineering, Sep. 1-2, 2000, Muju, Korea.

[23] Bertin, J. J., Bertin, R. S. and Yung, A., "The Launch-Tube Flow-Field for a Vertical Launching System," AIAA Paper 88-0332.

[24] K.S. Lee, S.K. Hong and S.O Park, "Improvements in Flux-Difference Splitting Algorithm for Accurate and Robust Flow Simulations," Computational Fluid Dynamics Journal, Vol. 10 No. 2 July 2001, pp. 181-191

[25] Richard Sanders, E. Morano, and M.C. Rduguert, "Multidimensional Dissipation for Upwind Schemes: Stability and Applications to Gas Dynamics," Journal of Computational Physics. 145, pp. 511-537, 1998.

[26] Quirk, J. J., "A Contribution to the Great Riemann Solver Debate," Intl. J. for Numerical Methods in Fluids, Vol. 18, pp. 555-574, 1994.

[27] Pandolfi, M, and D'ambrosio, D., "Numerical Instabilities in Upwind Methods: Analysis and Cures for the 'Carbuncle' Phenomenon," J. of C. P. 166, pp. 271-301, 2001.

[28] Lombard, C. K., Oliger, J., Yang, J. Y. and Davy, W. C., "Conservative Supra-Characteristics Method for Splitting the Hyperbolic Systems of Gasdynamics with Computed Boundaries for Real and Perfect Gases," AIAA-82-0837, June 1982.

[29] Hong, S. K., Bardina, J., Lombard, C. K., Wang, D. and Codding, W., "A Matrix of 3-D Turbulent CFD Solutions for JI Control with Interacting Lateral and Attitude Thrusters," AIAA 91-2099, Sacramento, June 1991.

[30] 홍승규, 이광섭, "Application of Characteristic Boundary Conditions in the Flux-Difference Splitting Framework," 대한기계학회 '99년도 유체공학부문 춘계학술강연회 강연집, pp. 141-156, 한양대학교, 1999. 5.

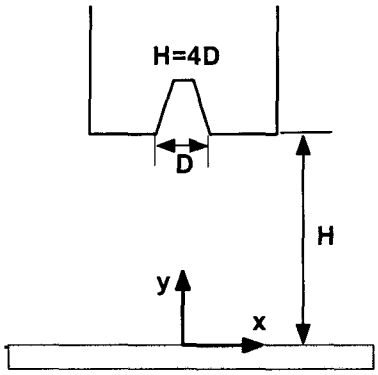

Fig. 1 Computational model.

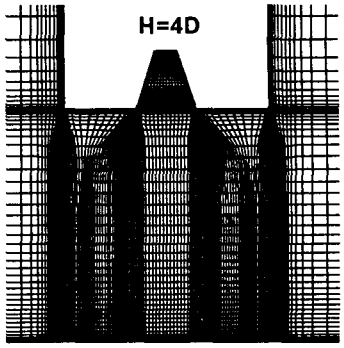

Fig. 2 Grid in symmetric plane.

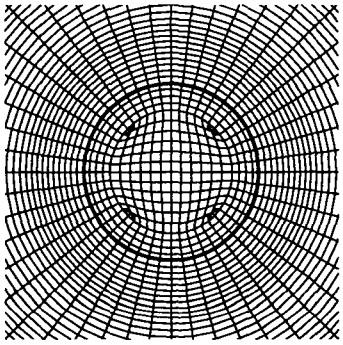

Fig. 10 Grid in transverse plane.

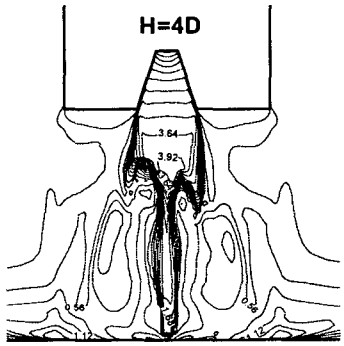

Fig. 4 Mach contours with conventional scheme.

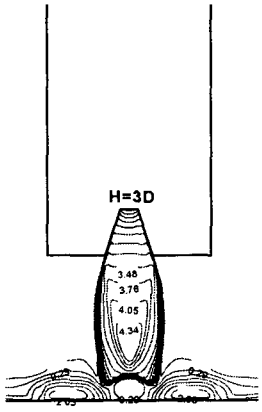

(a) H=3D

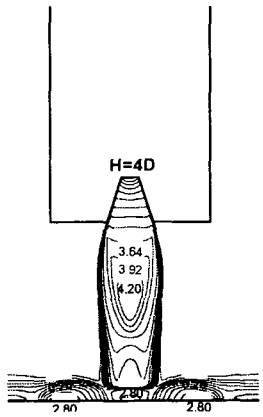

(b) H=4D

Fig. 5 Mach contours in symmetric plane for varied distance H.

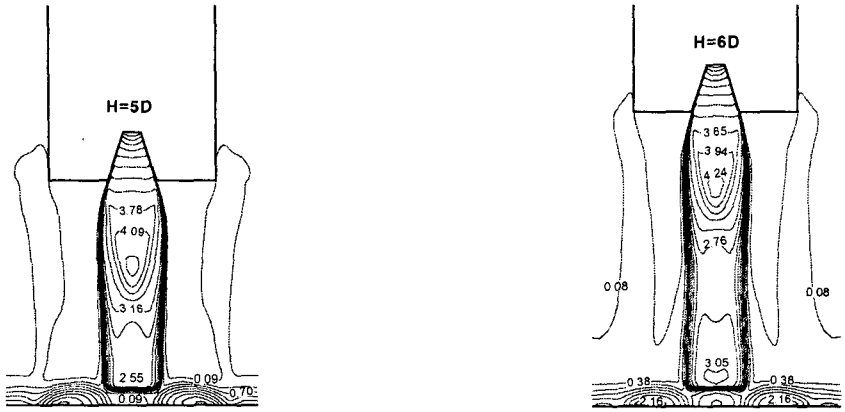

(c) H=5D (d) H=6D

Fig. 5 Mach contours in symmetric plane for varied distance H.

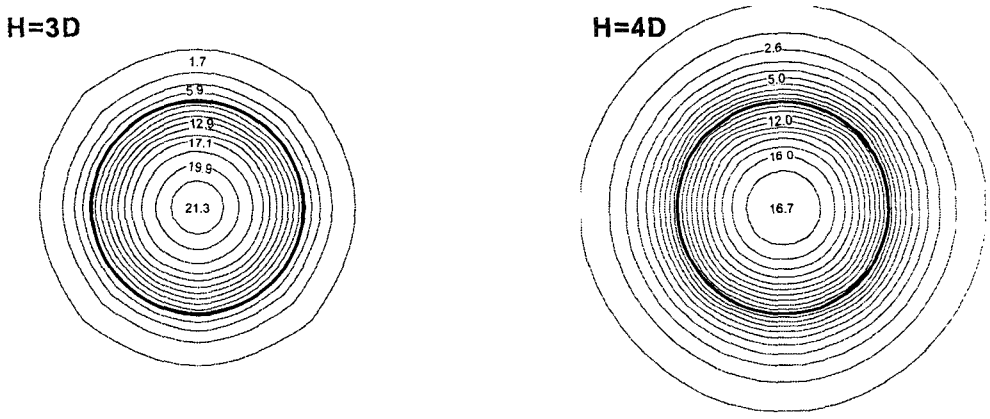

(a) H=3D (b) H=4D

Fig. 6 Pressure distributions on the flat plate (atm.)

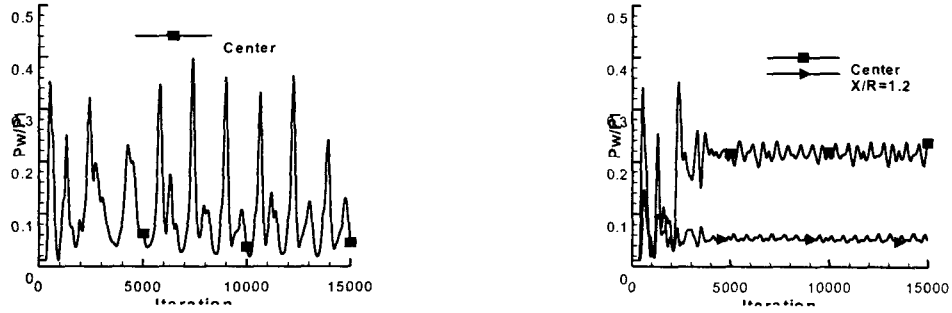

(a) H=3D (b) H=4D

Fig. 7 Pressure history for varied distance H.

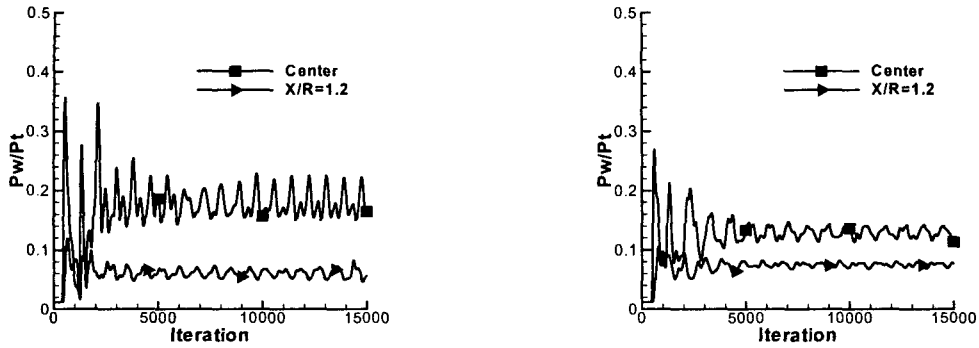

Fig. 7 Pressure history for varied distance H.

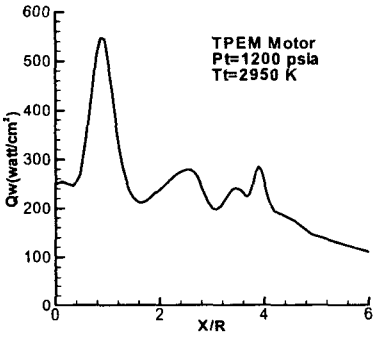

Fig. 8 Heat flux distributions in radial direction for H=4D.

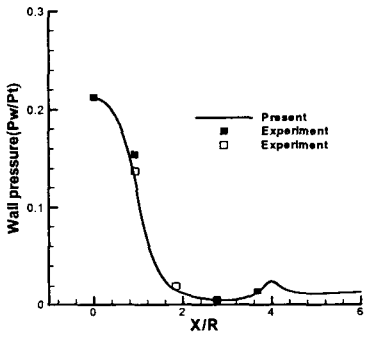

Fig. 9 Pressure distributions in radial direction for H=4D.

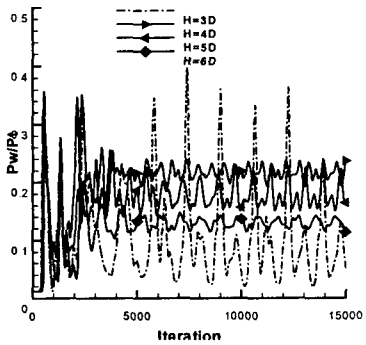

Fig. 10 Pressure history comparisons.

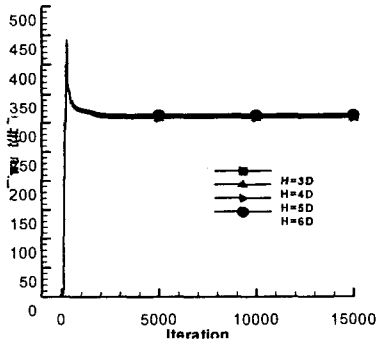

Fig. 11 Thrust history comparisons.